

SUPPORTING INFORMATION

Fabrication of 3D concentric amphiphilic microparticles to form uniform nanoliter reaction volumes for amplified affinity assays

Ghulam Destgeer,[†] Mengxing Ouyang,[†] Chueh-Yu Wu and Dino Di Carlo*

Abstract: Reactions performed in uniform microscale volumes have enabled numerous applications in the analysis of rare entities (e.g. cells and molecules). Here, highly monodisperse aqueous droplets are formed by simply mixing microscale multi-material particles, consisting of concentric hydrophobic outer and hydrophilic inner layers, with oil and water. The particles are manufactured in batch using a 3D printed device to co-flow four concentric streams of polymer precursors which are polymerized with UV light. The cross-sectional shapes of the particles are altered by microfluidic nozzle design in the 3D printed device. Once a particle encapsulates an aqueous volume, each “dropicle” provides uniform compartmentalization and customizable shape-coding for each sample volume to enable multiplexing of uniform reactions in a scalable manner. We implement an enzymatically-amplified immunoassay using the dropicle system, yielding a detection limit of <1 pM with a dynamic range of at least 3 orders of magnitude. Multiplexing using two types of shape-coded particles was demonstrated without cross talk, laying a foundation for democratized single-entity assays.

TABLE OF CONTENTS

<i>1. Laminar Flow and Diffusion Simulation</i>	2
<i>2. Droplet Characterization</i>	2
<i>3. 3D Device Design</i>	2
<i>4. Particle Manufacturing Setup</i>	3
<i>5. Materials for Particle Fabrication</i>	3
<i>6. Experimental Conditions for Particle Fabrication</i>	4
<i>7. Multi-material Particle Characterization</i>	4
<i>8. Particle Retention Rate</i>	5
<i>9. Costs and Scalability</i>	5
<i>10. Analysis of distinguishable shape codes</i>	6
<i>11. Direct Binding of Streptavidin to Particles</i>	6
<i>12. Supporting Figures</i>	7
<i>13. Supporting Table</i>	16

1. Laminar Flow and Diffusion Simulation

The laminar fluid flow inside the 3D printed devices and diffusion of the PI across the streamlines are simulated by coupling “Laminar Flow” and “Transport of Diluted Species” modules in COMSOL Multiphysics, MA, USA (Figure S2). A single phase fluid (density 987 kg/m^3 and viscosity $30 \text{ mPa}\cdot\text{s}$) flow is solved for as a stationary case. The viscosity of the fluid is assumed to be constant throughout the fluid domain, whereas a diffusion coefficient value of $10^{-10} \text{ m}^2/\text{s}$ for the PI is used. The inlet boundary conditions are set as laminar flow rates of 0.25 ml/min for all the inlets, whereas the outlet boundary condition is set at atmospheric pressure (0 Pa). Symmetric boundary conditions are used wherever applicable. The solution time for this problem with a 3D fluid domain is approximately 2 hrs on a computer with 8GB RAM and 2.33 GHz Core 2Duo processor. The experimental viscosities of the density matched PEGDA in ethanol and PPGDA in ethanol solutions are measured as $7.55 \text{ mPa}\cdot\text{s}$ and $38.3 \text{ mPa}\cdot\text{s}$, respectively. However, solving a two-phase flow, with different viscosities for each fluid, by coupling the “Laminar Two-Phase Flow, Phase Field” and “Transport of Diluted Species” modules is computationally expensive for a 3D geometry. Therefore, we instead solve a 2D axisymmetric case including the viscosity differences in the fluids. The results of this simulation showed a reasonable agreement in diffusion characteristics of the PI across the microchannel width. The solution time for the axisymmetric problem is more than 20 hrs. For brevity, the results for the axisymmetric case are not reported here.

The shapes of the fabricated particles match well with simulation results predicting the PI concentration distribution across the channel width and the location of the streamlines corresponding to each polymer precursor (Figure S2B, Figure S3). Diffusive blurring of the PI distribution leads to smoothening of sharper gradients of PI and better reflects the actual particle morphologies (Figure S2B). However, these blurred shaped particles do not affect the performance of the assay. Moreover, to overcome the effect of diffusive blurring and achieve better particle definition, the outer and inner sheath flow are replaced with inert non-crosslinkable precursors mixed with similar concentrations of PI. Therefore, the shape of the particles is less effected by the diffusion and is more accurately defined by the fluid streamlines as indicated in Figure S3.

2. Droplet Characterization

It is estimated that the O, H, Plus, and U shapes held approximately 2.8, 3.5, 4.1, and 2.9 nanoliters, respectively, largely due to differences in their internal PEG layer geometry (Figure S2C, Figure S2E). We also estimate the uniformity in drop size by calculating the variation in intensity of an encapsulated fluorophore. We calculated the drop volume for seven different O shaped particles with varying diameters and thicknesses, and obtained a CV of 9.3% on average. Assuming a spherical shape for a droplet this would only correspond to an approximately 3% CV in droplet diameter.

3. 3D Device Design

A 3D microfluidic device, having four inlet ports and one outlet port, is designed in AutoCAD (AutoDesk, CA, USA). Different devices are designed separately with various cross-sections of the channels for similar-shaped particles fabrication (Figure 2, Figure S3). The inlet ports lead to four stacked microfluidic channels ($635 \mu\text{m}$) separated by a thin wall ($400 \mu\text{m}$). All the channels are sequentially merged together within a 3-4.5mm long tapered region close to the outlet port, where the outer most dimension is reduced from $\sim 9 \text{ mm}$ to $\sim 0.7 \text{ mm}$. First the inner most channel is joined with the adjacent channel by removing the first wall in between them. As the cross-sectional dimension of the tapered region reduces further, the next channel is joined with the first two by removing the second wall in between them. Finally, when the tapered region converges close to the outlet port dimension, the fourth channel is also merged together with the first three channels. At the exit of the 3D printed part, the outlet cross-section is designed as a tapered square shape ($0.7 \text{ mm} \times 0.7 \text{ mm}$ to $1 \text{ mm} \times 1 \text{ mm}$) so that a square glass capillary (ID 0.5 mm , OD 0.7 mm) could be easily fit and align with the co-axial channels. The inlet ports have a diameter of

1.58 mm to tightly connect with the Polytetrafluoroethylene (PTFE) tubing with OD 1.58 mm. The microfluidic device is 3D printed using a photopolymer (WaterShed XC 11122, ProtoLabs, MN, USA) and a high-resolution (50 μm layers) stereolithography technique (ProtoLabs, MN, USA). The square glass capillary (8250, 50 mm, VitroCom, NJ, USA) and the PTFE tubing (Kimble, OD 1.58 mm and ID 0.78 mm, DWK Life Sciences, Germany) are glued (Devcon 5-Minute Epoxy 20845, ITW Consumer, CT, USA) to the 3D printed part ($\sim 11\text{ mm} \times \sim 15\text{ mm} \times \sim 21\text{ mm}$) and placed on top of a stack of supporting glass slides. A Luer stub blunt needle (LS21, Instech Laboratories, PA, USA) is also glued at the end of the glass capillary.

4. Particle Manufacturing Setup

The 3D printed microfluidic device connected to a glass capillary is fixed on top of a custom-built stage. The inlet ports are connected (PEEK Union Assembly P-702, OD 1.58 mm, IDEX, IL, USA) to four syringes (20 ml Plastic Syringe with Luer-Lok Tip, BD, NJ, USA) mounted on two separate syringe pumps (PHD 2000, Harvard Apparatus, MA, USA) using PTFE tubing and Luer stubs. PTFE tubing from the outlet Luer stub is passed through a pinch valve (2-Way Pinch Valve, P045104L0A00F1, ASCO, NJ, USA) into a collection vessel (conical tubes, Corning, NY, USA). A photomask (Chrome Film Mask, CAD/Art Services, OR, USA) is taped on top of the glass capillary to provide a controlled UV exposure. A UV source (OmniCure S2000, Excelitas Technologies, MA, USA) exposes the capillary's region of interest under the photomask through a light guide with a collimator (Adjustable Spot Collimating Adaptor, Excelitas Technologies, MA, USA) and a light shutter (Lambda SC, Smart Shutter control system, Sutter Instrument, CA, USA) attached at its end. The syringe pumps, valve and shutter are automated and controlled using a graphical user interface developed in LabVIEW (National Instruments, TX, USA).

5. Materials for Particle Fabrication

For the hydrophilic and hydrophobic layers of the multi-material 3D particles, poly(ethylene glycol) diacrylate (PEGDA, $M_w \approx 575$; 437441, Sigma-Aldrich, MO, USA) and poly(propylene glycol) diacrylate (PPGDA, $M_w \approx 800$; 455024, Sigma-Aldrich, MO, USA) are chosen to be the polymer precursors, respectively. The densities of the PPGDA (1.01 g/cm^3) and PEGDA (1.12 g/cm^3) solutions are matched (0.987 g/cm^3) by adding 10% and 40% ethanol (0.789 g/cm^3) in the mixtures, respectively. The photoinitiator (PI) concentration for channel 2 and 3 is maintained at 5% of the total volume of the PPGDA (90%) in ethanol (10%) and PEGDA (60%) in ethanol (40%) mixtures, respectively. For flow configuration 1, the photoinitiator (2-hydroxy-2-methylpropiophenone, Darocur 1173, 405655, Sigma-Aldrich, MO, USA) is added only to the two precursors that are to be polymerized upon UV exposure, when the outer and inner sheath flows are PPGDA and PEGDA, respectively. However, for flow configuration 2, to reduce the effect of PI diffusion on particles blurring, the outer and inner sheath flows are replaced with PPG ($M_w \approx 400$; 81350437441, Sigma-Aldrich, MO, USA) mixed with PI and PEG ($M_w \approx 200$; P3015, Sigma-Aldrich, MO, USA) mixed with PI, respectively. For the biotin to streptavidin-HRP binding assays reported, the inner PEGDA layer is also biotinylated to enable binding of streptavidin. Before the particle fabrication, 0.25 ml of acrylate-PEG-biotin (APB, PG2-ARBN-5k, NANOCS, NY, USA) dissolved in DMSO (100 mg in 1.66 ml) is mixed with 20 ml of PEGDA and ethanol solution. The biotin is grafted within the PEGDA layer during photo-crosslinking.

For a final concentration of 0.75 mg of APB per ml of PEGDA solution, we can estimate 9.033×10^{16} APB molecules/ml or 9.033×10^{22} APB molecules/ m^3 . A 5 kDa APB molecule has an approximate 1.1 nm radius of gyration or 2.2 nm diameter. An APB molecule would be available for binding if it is present within a thickness of $< 2.2\text{ nm}$ from the particle's inner cavity surface exposed to the aqueous phase. For an O-shaped amphiphilic particle with a cavity diameter of 200 μm , and thickness of 100 μm , we estimate

the number of APB molecules present within a 2 nm (< 2.2 nm molecular diameter) PEGDA width to be $\sim 1.1 \times 10^7$ per particle.

6. Experimental Conditions for Particle Fabrication

Production conditions for example O-shaped particles shown in Figure 1F are provided. Particles were fabricated by pumping the polymer precursors through the four separate inlets of the 3D printed device at flow rates of 0.25 ml/min each, where $\tau_d = 1.25$ s, $\tau_{exp} = 0.3$ s, and $\tau_s = 4$ s. A net flow rate of 1 ml/min results in $U_{avg} = 66.7$ mm/s, Reynolds number $Re \cong 1.4$ and Peclet number $Pe = 3.3 \times 10^5$ for a glass capillary with hydraulic diameter of $d_h = 0.5$ mm. For a UV exposure length of ~ 10 mm, it takes $t \cong 0.15$ s for a fluid particle to travel such a distance. Therefore, the diffusion length $L_D = \sqrt{Dt}$ for the PI molecules is calculated as $3.9 \mu\text{m}$ with a diffusion coefficient $D = 10^{-10}$ m²/s. Diffusive blurring at this length scale results in a minor variation ($< 1\%$) in the PI concentration profile compared to the microchannel width (~ 0.5 mm) and length (~ 10 mm). Conditions for manufacture of other particles used are described in the Supporting Information.

The experimental conditions for the manufacture of the particles using flow configuration 1 described in Figure S2C are as follows: for O-shaped particles, $\tau_{exp} = 0.3$ s, $\tau_d = 1.25$ s, $\tau_s = 4$ s, and total flow rate ($Q_t = Q_1 + Q_2 + Q_3 + Q_4$) = 1 ml/min, $Pe = 3.3 \times 10^5$; for plus-shaped particles, $\tau_{exp} = 0.3$ s, $\tau_d = 1.75$ s, $\tau_s = 2$ s, and $Q_t = 2$ ml/min, $Pe = 6.6 \times 10^5$; for H- and U-shaped particles, $\tau_{exp} = 0.3$ s, $\tau_d = 2.25$ s, $\tau_s = 4$ s, and $Q_t = 1$ ml/min, $Pe = 3.3 \times 10^5$. The average inner dimensions of the particles for the above experimental conditions are measured as $187.6 \pm 6.7 \mu\text{m}$, $209.9 \pm 5.7 \mu\text{m}$, $228.7 \pm 2.6 \mu\text{m}$, and $194.4 \pm 6.1 \mu\text{m}$ for O-, H-, Plus-, and U-shaped particles, respectively. The flow rates ratios are kept constant for these experiments ($Q_1 = Q_2 = Q_3 = Q_4 = 1$). It is worth noting that the flow stabilization time could be reduced to half, $\tau_s = 2$ s, if the flow rate is doubled ($Q_t = 2$ ml/min). The experimental conditions corresponding to the four different flow rate ratios of 1 to 4 in Figure S2D are as follows: $\tau_{exp(1-4)} = 0.3$ s, $\tau_{d(1-4)} = 1, 1.25, 1.5, 1.75$ s; $\tau_{s(1-4)} = 4$ s, and $Q_{t(1-4)} = 1, 1.5, 2, 2.5$ ml/min. The experimental conditions for fabrication of particles used in assay experiments (Figure 5) are as follows: (design 1) PI concentration of 5%, $\tau_{exp} = 0.3$ s, $\tau_d = 1$ s, $\tau_s = 4$ s, and $Q_t = 1$ ml/min ($Q_{1,2} : Q_{3,4} = 1$), particle's thickness defined by the mask width $t = 200 \mu\text{m}$; (design 2) PI concentration of 5%, $\tau_{exp} = 0.3$ s, $\tau_d = 1.75$ s, $\tau_s = 2$ s, and $Q_t = 2$ ml/min ($Q_{1,2} : Q_{3,4} = 1$), $t = 100 \mu\text{m}$. The experimental conditions for the manufacture of the particles with flow configuration 2 described in Figure 2 are as follows: $\tau_{exp} = 0.5$ s, $\tau_d = 1.5$ s, $\tau_s = 4$ s, and $Q_t = 1.5$ ml/min, $Pe = 4.95 \times 10^5$.

7. Multi-material Particle Characterization

The particles collected directly from the device after a complete fabrication cycle are initially suspended in a mixture of uncured PEGDA and PPGDA in ethanol. Additional ethanol is added to reduce the overall density of the solution so much so that the particles becomes heavier than the media and settle on the bottom of the conical sample collection tube. After removing the supernatant, the particles are washed with pure ethanol three times with $>100\times$ volume and are stored in ethanol for later experiments. For PEGDA layer visualization, the particles are transferred from ethanol to phosphate-buffered saline (PBS) after three washing steps. The particles are incubated with resorufin dissolved in PBS buffer (100 μM solution) for ~ 10 min. After washing the excess resorufin away with PBS ($\times 3$), resorufin partitioned into the PEGDA layer only is observed in the TRITC channel of the fluorescence microscope images. For characterization of particle dimensions, the fabricated particles suspended in ethanol are dispersed in a 12-well plate (Falcon untreated cell culture plates, Corning, NY, USA), where images are captured using a microscope and image analysis is performed using ImageJ (NIH, MD, USA). By adjusting the threshold, the inner and outer boundaries of each particle are identified, and the areas encompassed by these boundaries are measured separately. Correlating the measured area to the area of a circle, average diameters are deduced that represent the inner and outer dimension of the particle. In some case, a band

pass filter is applied to the images before applying the threshold that helps in clearly identifying the boundaries of the particles.

8. Particle Retention Rate

For 300-600 seeded particles in a 12 well plate more than 98% of particles can be retained after the washing steps (data examined for five different experiments). To calculate the retention rate, the number of seeded particles were counted in ethanol and later in PBS, after all the washing steps were performed. High retention rates reflect the density differences between the multi-material particles and the surrounding media, and the exchange of media using gentle pipetting techniques without excessive agitation. When the particles are initially transferred to the well plate in ethanol, they naturally settle on the surface due to the slightly higher material densities (1.12 g/ml for PEGDA and 1.01 g/ml for PPGDA) compared to ethanol (0.789 g/ml). In the later assay steps such as biomolecule incubation and washing steps, conducted in aqueous solution (typically PBS, 1.005 g/ml), these particles with hydrophobic outer layers prefer the hydrophobic surface of the well plate in PBS, so they are not lost during the washing steps. Moreover, during the solution transfer steps, the solutions were gently added to the center of the well, and excess solutions were removed from the corner of the well. As the fluid is sucked from the corner side of the well, the induced shallow boundary layer flow profile does not exert a significant drag force to disrupt the already settled particles from their positions. For a higher seeding density, we observe 94.3% retention rate when the particles are transferred from ethanol to PBS and washed three times as shown in Figure 3 (1048 particles in ethanol, 989 particles in PBS), where the whole well image of hundreds of particles is monitored at different steps. In the inset images, the particles retained similar locations and orientations throughout the process. Finally, when the oil (1.05 g/ml) is added for encapsulation, it is absorbed by the outer hydrophobic polymer layer of the particle as well as priming the hydrophobic well surface. The low interfacial tension between the particles and the continuous phase prevents the particles from sticking to each other. However, the particles stay settled at the bottom of the well, presumably because of the density differences as described above and the viscous nature of the oil that dampens any significant movements of the particles after the droplets are formed. These particle handling and medium exchange steps are very similar to the steps for conducting cell-based assays in a well plate, where excessive agitation is in general avoided to minimize unnecessary cell loss. On the other hand, we did observe that if agitation of the well plate is applied after droplet formation, the particles with droplets could be easily retrieved and transferred to another well or tubes as desired, which adds to the flexibility of downstream analysis.

9. Costs and Scalability

The pure polymer precursors, PPG, PPGDA, PEGDA, and PEG cost ~\$78, ~\$185, ~\$180, and ~\$25 per liter each. The density matched mixtures in ethanol (~\$5/L) cost ~\$71, ~\$167, ~\$110, and ~\$17 per liter, respectively, averaging at ~\$91/L. An addition of 5% PI (\$1/mL) in each of the precursors cost ~\$141/L on average. For an overall flow rate of 1 mL/min (i.e. 0.25 mL/min for each stream) and a continuous 4s of pumping after each UV exposure to create ~30 particles per cycle, it takes ~2.2 μ L of reagents per particle fabricated. A liter of reagents can be easily transformed into $\sim 2.2 \times 10^6$ particles. Therefore, more than 15,000 particles can be easily fabricated with ~\$1 worth of reagents. Particles are manufactured in a continuous and automated manner which is scalable to large batches. The throughput of particle production is less important than the throughput of drop generation for microfluidic droplet assays because for microfluidic assays the total assay time includes the time to produce the assay droplets. Production time for particles occurs separately and is decoupled from the time to produce droplets. Droplet formation occurs rapidly in less than 1 minute for an entire well filled with particles.

10. Analysis of distinguishable shape codes

An estimation on the number of shape-codes that could be achieved based on circularity and sizes of the particles are conducted with measured particle CVs as a reference for the increment distinguishable. For particles with similar overall sizes, assuming a circularity range of 0.4-0.9, and a 0.05 resolution/interval (current CV on circularity is ~2.5% on average, i.e., ~0.025 in circularity), this would lead to 10 separate particle types that are distinguishable. For particles with the same shape, assuming an outer diameter range of 300-400 μm and inner diameter range of 100-200 μm (based on the particles reported in the current manuscript), and 20 μm resolution/interval (current CV on outer diameter is <2%, i.e., <8 μm , and on inner diameter <4%, i.e. <8 μm), this would lead to 5 distinguishable particle types. Therefore, just combining modulation in particle sizes and circularities, $5 \times 10 = 50$ different shape-codes can be established. With further improvement of the fabrication process to achieve a wider range of particle sizes and smaller CVs, as well as the implementation of different shape-coding strategies beyond circularity and size changes, we expect to expand the shape-coded particle library significantly.

11. Direct Binding of Streptavidin to Particles

To evaluate signal from direct binding, particles (design 2) are transferred to a well plate and washed in the same manner as above followed by incubation with streptavidin-Alexa Fluor[®] 568 (Thermo Fisher Scientific, MA, USA) at varying concentrations for 30 min, which is the same duration as for the amplification reaction, then three washes in PBSP. Next, droplets were formed by adding oil. In the negative control group, particles were incubated with PBS only and all the other steps were kept the same as the positive groups. Fluorescence (TRITC) images were obtained in the same manner as the amplified assay with 40ms exposure time. Due to direct labeling, the fluorescent signal is generated from the biotin-streptavidin-Alexa Fluor[®] 568 complex, largely localized in the PEG layer. For imaging analysis, ROIs are defined as both the PEG layer and the internal droplet, the averaged signal from the ROI is used to represent the signal from that particle.

12. Supporting Figures

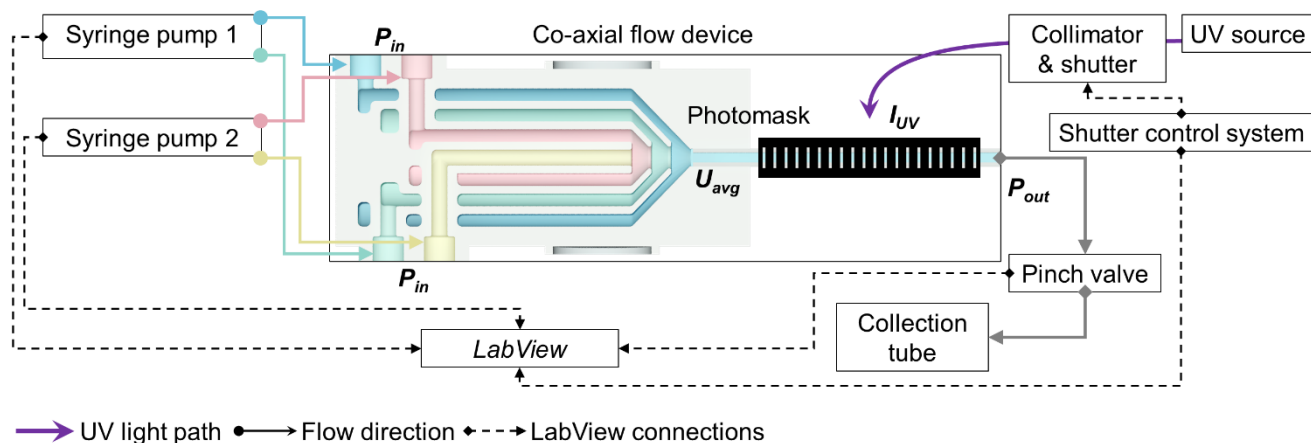


Figure S1. Stop flow lithography setup. The co-axial flow device is connected to two syringe pumps at the inlet and a collection tube at the outlet through a pinched valve. UV source shines light on the device through a collimator and shutter to curable precursors under the photomask. The pumps, the pinch valve and the shutter control system are connected using LabView and controlled in an automated manner from a computer.

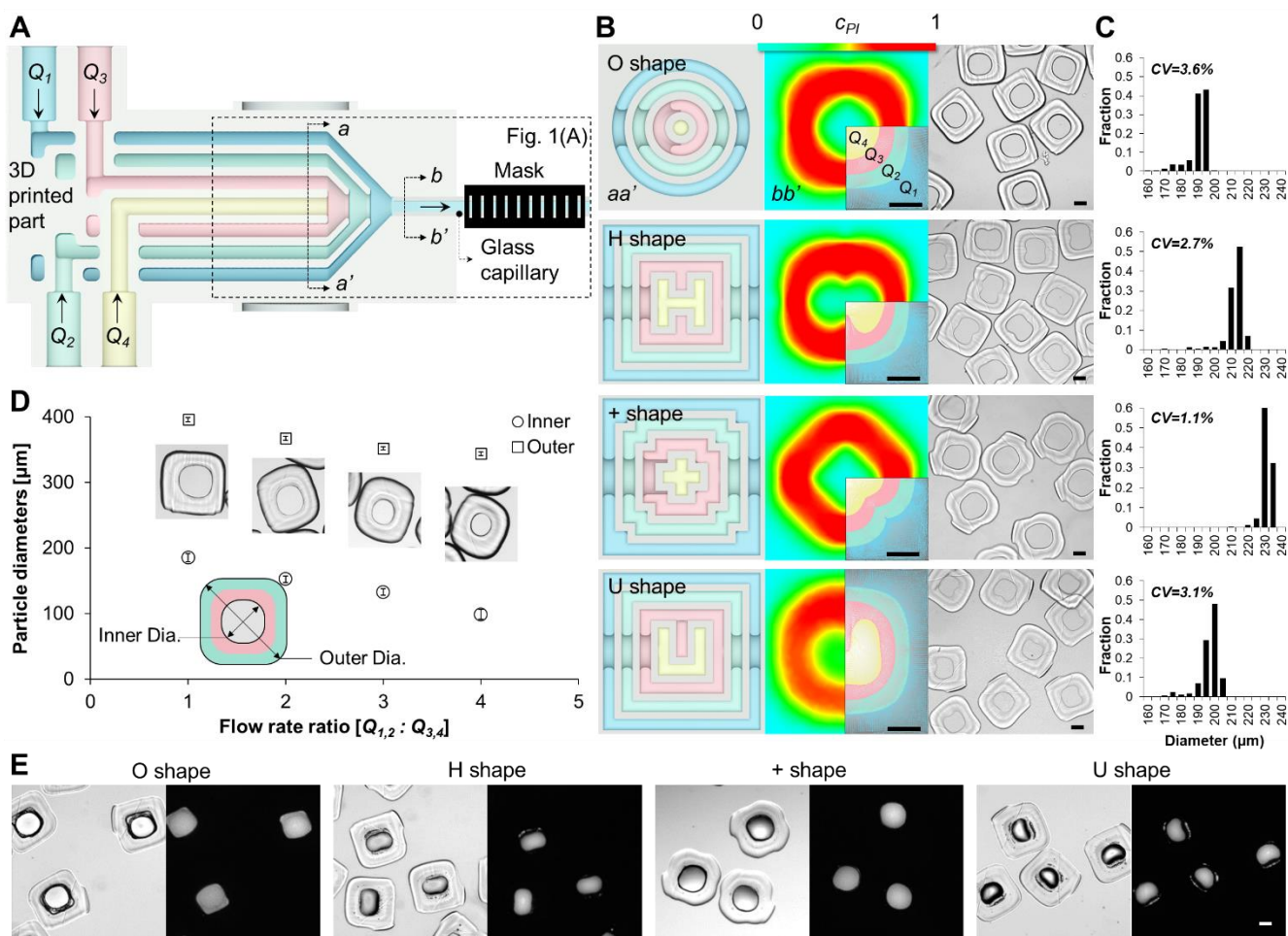


Figure S2. Shape-coded particles. (A) A cross-section of the 3D printed part joined with a square glass capillary is shown. The inner surfaces of the channels are colored blue, green, red and yellow to demonstrate they carry the four matching fluid streams (Q_{1-4}) (see Figure 1A). (B) (left) The cross-section $a-a'$ of the device in (A) is shown for four different designs (O, H, Plus, and U shapes). (center) For the same designs, simulations of the concentration of PI (c_{PI}) across the channel width at section $b-b'$ are shown for a laminar flow. The heat-maps show the normalized c_{PI} across the channel width when solving a convection diffusion equation. The insets show the location of the streamlines associated with each inlet flow Q_{1-4} within the square capillary cross-section (i.e. no diffusive blurring). (right) Manufactured particles corresponding to O, H, Plus and U-shape channel designs are shown. Scale bars are 100 μm . (C) For each channel design, there is a narrow distribution in inner diameter of the cavities for manufactured particles. (D) Inner and outer diameters of O-shaped particles as depicted in the inset schematic are plotted against the flow rate ratios ($Q_{1,2} : Q_{3,4}$). (E) Bright field and fluorescence images show FITC-containing aqueous droplets trapped within the cavities of the four different particle shapes (O, H, Plus, and U). Scale bar is 100 μm .

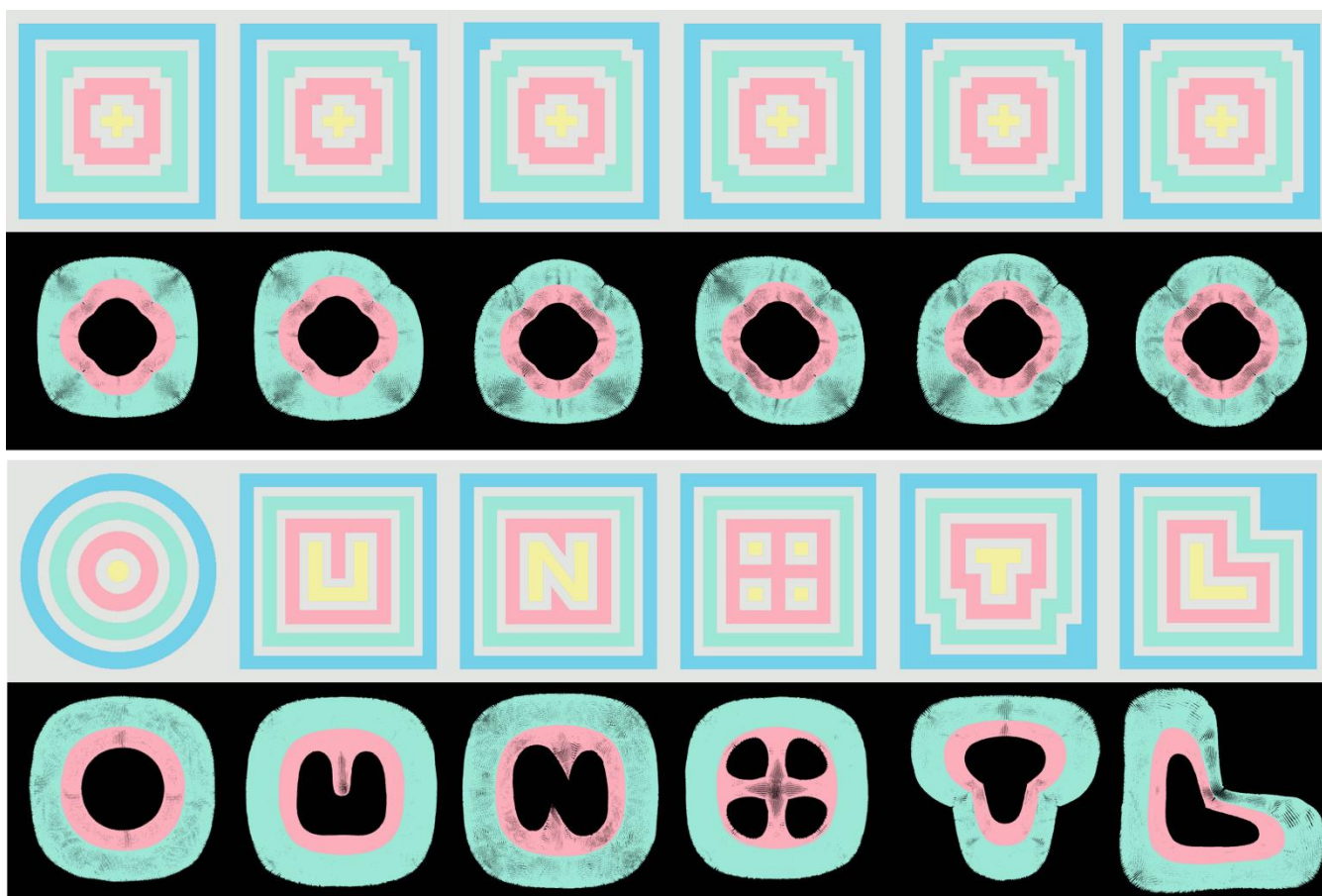


Figure S3. Shape coded 3D printed devices and simulated streamlines. Device cross-sections at a-a' as indicated in Figure S2A and simulations of cross-sections of fluid streamlines corresponding to particles manufactured in Figure 2 are shown. The first and third row show the 3D printed device cross-sections and second and fourth row show the corresponding streamlines for flows through the device immediately above the simulation. The flow rate ratios for the simulations are $Q_{1,2} : Q_{3,4} = 2:1$. The cyan and magenta colored streamlines indicate the location of curable PPGDA and PEGDA streamlines respectively.

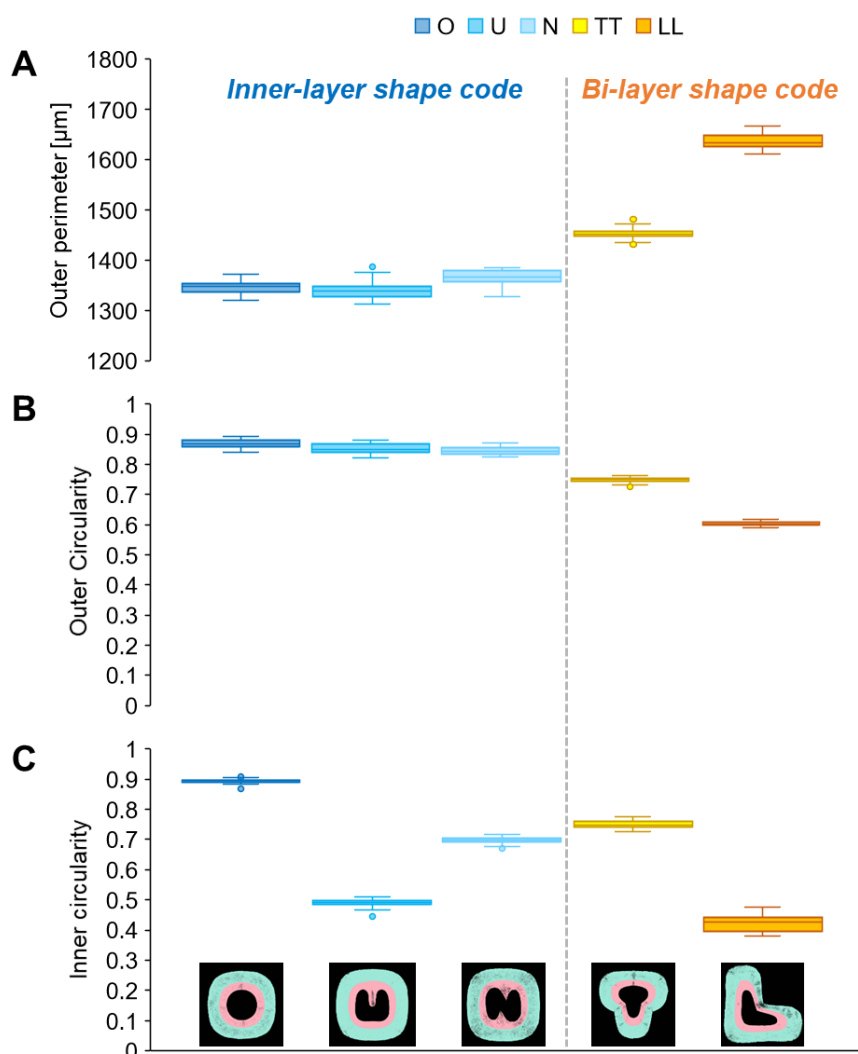


Figure S4. Analysis of particle size and circularity to distinguish different shape codes. Five different particle designs were analyzed including O, U, N, TT and LL shapes (Figure 2 and Figure S3). In the first three designs, the inner-layer is shape coded as the outer boundary stays constant. The latter two designs are bi-layer shape coded with T and L shapes, respectively. The particles can be categorized into inner-layer (blue) and bi-layer (yellow) shape codes using outer perimeter and circularity. Then, within the same category, the particles can be further differentiated based on their inner circularity. **(A)** The outer perimeters of the O, U and N particles using inner-layer shape codes are similar because of the square-like outer boundaries (mean values of 1345, 1339 and 1367 μm , respectively). However, the TT and LL particles have clearly distinct perimeters (mean values of 1453 and 1637 μm , respectively), which are larger than that of the O, U and N shapes. The CVs for all of these measurements are $\sim 0.9\%$ on average. Total number of particles analyzed, $N = 306$. **(B)** The outer circularities of the inner-layer shape codes, i.e. O, U and N, are similar for the same reason (mean values of 0.87, 0.85 and 0.85, respectively). However, the bi-layer shape codes, i.e. TT and LL, have relatively smaller outer circularities (mean values of 0.75 and 0.60, respectively), which clearly put them apart from the rest of the inner-shape codes, and moreover, provide a distinction between bi-layer shape codes. The CVs for all these measurements are $\sim 1.4\%$ on average. Total number of particles analyzed, $N = 306$. **(C)** The inner-layer shape codes can be separately identified by their inner circularities, i.e. mean values of 0.89, 0.49 and 0.70 for O, U and N shapes, respectively. The bi-layer shape codes can independently be distinguished from the inner circularities as well with mean values of 0.75 and 0.42 for TT and LL shape codes, respectively. The CVs for these measurements are $\sim 2.5\%$ on average. Total number of particles analyzed, $N = 287$.

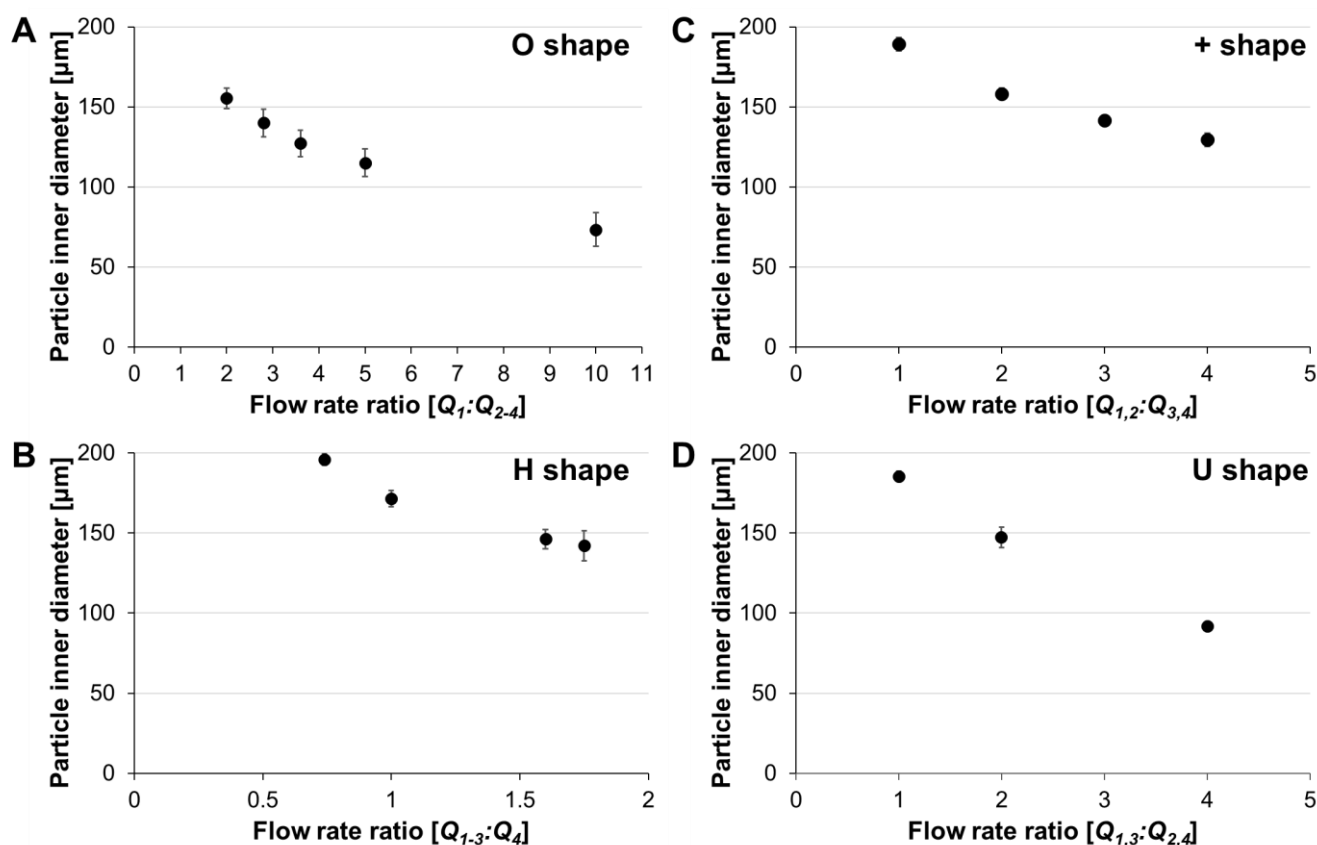


Figure S5. Modulation of particle inner diameter as a function of flow rate ratios for four different particle shapes. (A) The size of the O-shaped particle cavity decreased gradually as the flow rate ratio ($Q_1 : Q_{2-4}$) increased from 2 to 10. The experimental conditions are as follows: PI concentration of 5%, $\tau_{exp} = 0.3$ s, $\tau_d = 1$ s, $\tau_s = 5$ s, and $Q_t = 1.25, 1.45, 1.65, 1.6, 1.3$ ml/min corresponding to each data point in the plot. (B) The size of the H-shaped particle cavity decreased gradually as the flow rate ratio ($Q_{1-3} : Q_4$) increased from 0.74 to 1.75. The experimental conditions are as follows: PI concentration of 5%, $\tau_{exp} = 0.5$ s, $\tau_d = 2.25$ s, $\tau_s = 4$ s, and $Q_t = 1$ ml/min for all the measurements. (C) The size of the plus-shaped particle cavity decreased gradually as the flow rate ratio ($Q_{1,2} : Q_{3,4}$) increased from 1 to 4. The experimental conditions are as follows: PI concentration of 5%, $\tau_{exp} = 0.3$ s, $\tau_d = 1, 1.25, 1.5, 1.75$ s, $\tau_s = 4$ s, and $Q_t = 0.6, 0.9, 1.2, 1.5$ ml/min, respectively, for the corresponding measurements. (D) The size of the U-shaped particle cavity decreased gradually as the flow rate ratio ($Q_{1,3} : Q_{2,4}$) increased from 1 to 4. The experimental conditions are as follows: PI concentration of 2 and 4% in PPGDA and PEGDA, respectively, $\tau_{exp} = 0.5$ s, $\tau_d = 1$ s, $\tau_s = 5$ s, and $Q_t = 1.2, 1.4, 1.6$ ml/min, for the corresponding measurements.

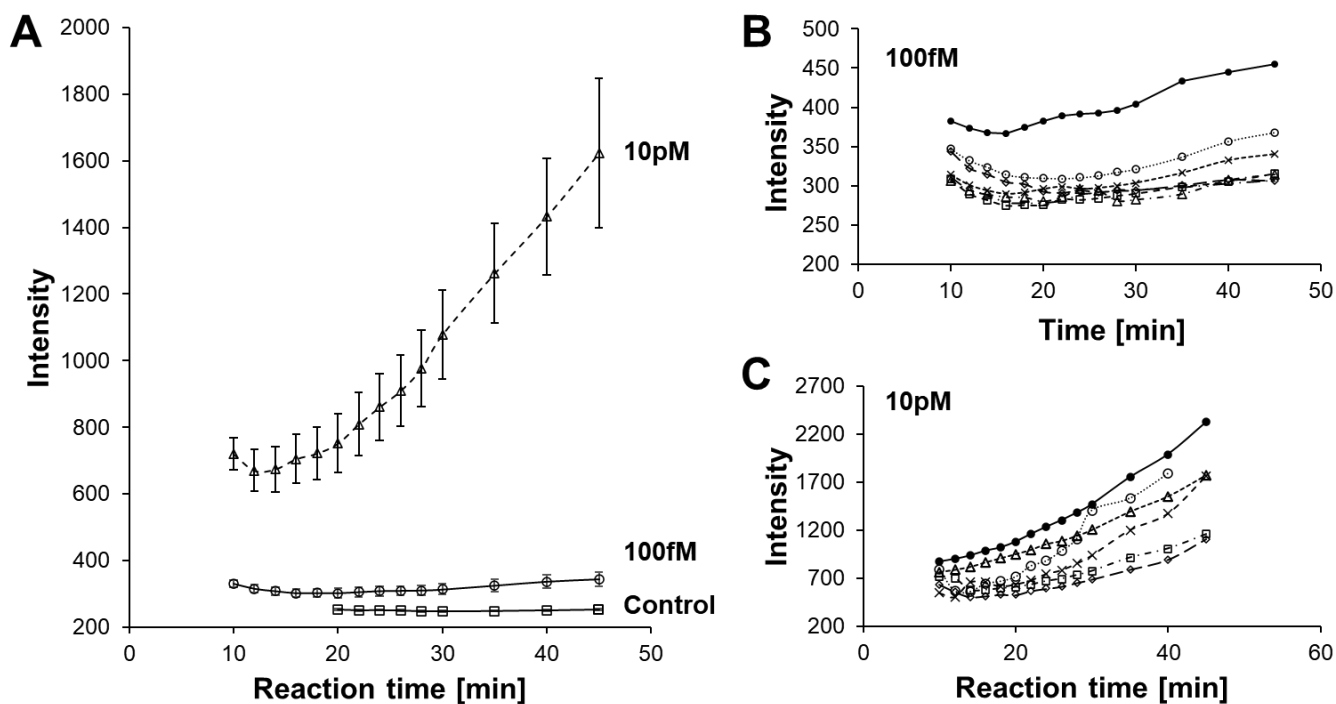


Figure S6. Time dependence of intensity change in droplets using a QuantaRed assay. (A) Fluorescence signal increase over time from 10 to 45 min for binding of biotinylated particles with streptavidin-HRP at 10 pM and 100 fM concentrations. The control condition is the same particles and reagents without streptavidin-HRP. Data represents mean of intensity for droplets with error bars representing standard error of the mean. Intensity drop at early time points is likely due to changes in shape/swelling upon introduction of the oil phase. **(B-C)** Fluorescence intensity from individual particles are shown over time for (B) 100 fM and (C) 10 pM concentrations of streptavidin-HRP respectively.

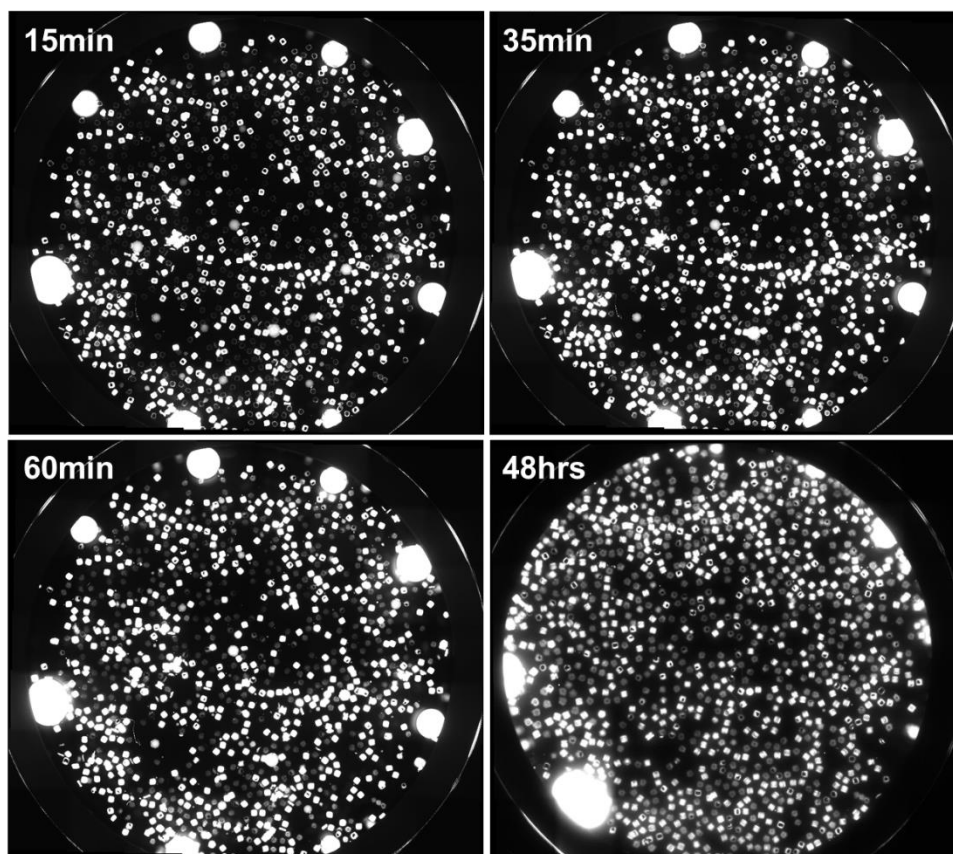


Figure S7. Minimal cross talk is observed between reactions in separate droplets over time. Microscopic images showing the same well at 15 min, 35 min, 60 min, and 48 hrs after initiating the QuantaRed reaction. Two types of particles (with and without biotin) are introduced and incubated with 0.1 nM of streptavidin-HRP.

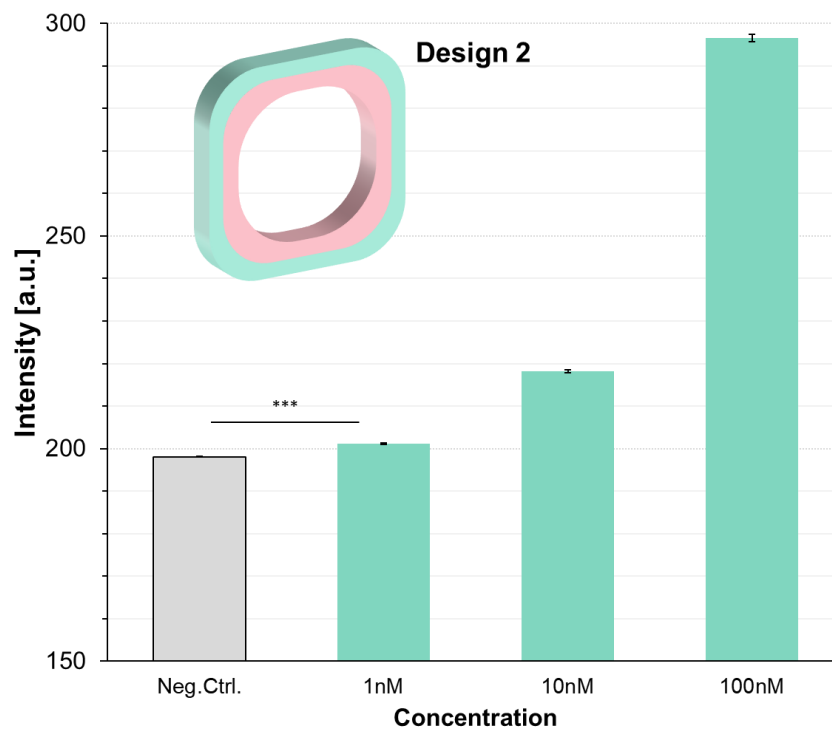


Figure S8. Direct binding assay using streptavidin. Intensity as a function of concentration for direct binding of fluorescent streptavidin without amplification using enzymes. Particles with design 2 are used. Error bars represent standard error. *** represents $p < 0.001$.

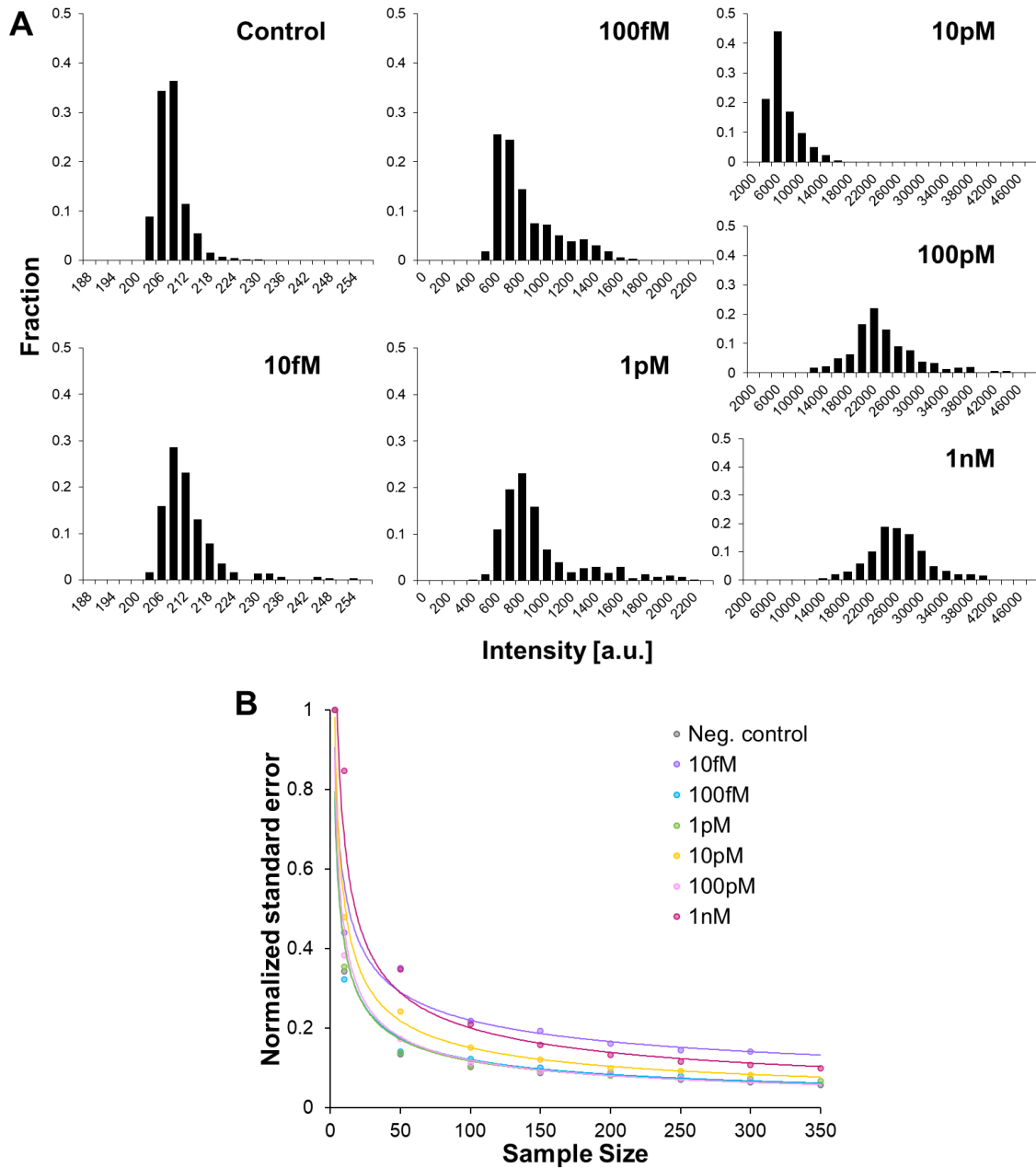


Figure S9. Swarm sensing with droplets. (A) Histograms of fluorescence intensities for populations of droplets formed from O-shaped particle design 2 after the QuantaRed assay readout at 45 min. Concentration of streptavidin-HRP ranges from 0 (control) to 1 nM. Results correlate with the mean intensity results reported in Figure 6C. (B) Normalized standard error of the mean vs number of droplets in the sample for the amplified assay showing that a larger number of droplets leads to a more accurate representation of the concentration of analyte.

13. Supporting Table

Table S1. Comparison of multi-material particle fabrication techniques.

	Techniques ^(a)	CFL	CFL	CFL	SFL	HFL	HFL	SFL	MLL	MLL	IFS	HFT	3D Co-flow
	Year	2006	2007	2007	2007	2010	2012	2014	2009, 2015	2012	2015-18	2018	2019
	Reference(s)	20	22	21	25	29	32	7	33,34	43	37,38,40	36	Current
Fabrication mechanism	Channel material^(b)	PDMS	PDMS	PDMS	PDMS	PDMS	PDMS	PDMS	PDMS	PDMS	PDMS	COC	WS
	Coating material^(c)	×	×	×	×	×	NOA81	PFPE	×	×	×	×	×
	O₂ inhibition layer	○	○	○	○	○	×	○	○	○	○	N/A ^(d)	×
	Inert flows	×	×	×	×	×	○	×	×	×	×	×	○
	Hydrodynamic focusing	×	×	×	×	○	○	×	○	×	○	×	○
	Organic solvents	×	×	×	×	×	○	○	×	×	×	×	○ ^(e)
Particle characterization	Particle size (~μm)	3	100	180-270	1-6	50	50-200	20-250	100	200	100-500	50	100-200 ^(f)
	3D shaped particles	×	×	×	×	×	×	×	○	○	○	○	○
	On-demand size control	×	×	×	×	×	×	×	×	×	○	×	○
	Amphiphilic particles	×	○	×	×	×	×	×	×	○	×	×	○
	Uniform Droplet formation	×	× ^(g)	×	×	×	×	×	×	×	○ ^(h)	×	○

^(a) CFL: Continuous Flow Lithography, SFL: Stop Flow Lithography, HFL: Hydrodynamic Flow Lithography, MLL: Maskless Lithography, IFS: Inertial Flow Sculpting, HFT: Hollow Fiber Template.

^(b) PDMS: Polydimethylsiloxane, WS: WaterShed XC 11122, COC: Cyclic olefin copolymer.

^(c) NOA81: Norland Optical Adhesive 81, PFPE: Perfluoropolyether.

^(d) O₂ inhibition mechanism unknown.

^(e) Data not shown.

^(f) Thickness of the particles based on UV exposure window size.

^(g) Droplet formed using multiple particles but lacked uniformity and controllability.

^(h) Uniform volumes formed using multi-material particles, but throughput was limited by the multi-step fabrication process.